Chemically bonded interface construction of covalent organic framework/$CsPbBr_3$ heterojunction for efficient photocatalytic CO_2 reduction driven by visible light

Min Zhou[1], Zhiqing Wang[3], Aohan Mei[1], Keqiang Chen[4], Jianrong Zeng[5], Yueli Liu[1,2*], Wen Chen[2, 3*]

[1] *State Key Laboratory of Silicate Materials for Architectures, School of Materials Science and Engineering, Wuhan University of Technology, Wuhan, 430070, P. R. China*

[2] *Sanya Science and Education Innovation Park, Wuhan University of Technology, Sanya, 572024, P. R. China*

[3] *State Key Laboratory of Advanced Technology for Materials Synthesis and Processing, School of Materials Science and Engineering, Wuhan University of Technology, Wuhan, 430070, P. R. China*

[4] *Faculty of Materials Science and Chemistry, China University of Geosciences, Wuhan 430074, P. R. China*

[5] *Shanghai Synchrotron Radiation Facility, Shanghai Institute of Applied Physics, Chinese Academy of Sciences, Shanghai, 201204 P. R. China*

[*]Corresponding author:

Yueli Liu

E-mail: lylliuwhu@hotmail.com

Wen Chen

E-mail: chenw@whut.edu.cn

1 Materials and characterizations

1.1 Materials Chemicals

$PbBr_2$(99.98%) and CsBr (99.99%) were purchased from Aladdin. 1,3,5-Benzenetricarboxaldehyde (Tp) and 2,2'-Bipyridine (Bpy) were purchased from Jilin Chinese Academy of Science-Yanshen Technology Co., Ltd. Acetic acid (99.5%) and HBr (40.0%) were obtained from the Sinopharm Chemical Reagent Co., Ltd. Acetonitrile (≥ 99.5%), mesitylene (98%) and 1,4-dioxane (≥ 99.5%) were purchased from Aladdin. All reagents were of analytical grade and used without further purification.

1.2 Determination of apparent quantum efficiency

The apparent quantum efficiency (AQE) of the reaction system was measured using a Xe lamp with light band-pass filter (PLS-SXE300D, Beijing Perfectlight). The irradiation area was 3.14* 2.25 cm^2 with the same irradiation distance. Depending on the amount of CO and CH_4 evolution, AQE was calculated as following:

$$AQE(CO)\ \% = 2 \times (nCO \cdot NA \cdot h \cdot c) / (I \cdot S \cdot t \cdot \lambda) \times 100\%$$

$$AQE(CH_4)\ \% = 8 \times (nCH_4 \cdot NA \cdot h \cdot c) / (I \cdot S \cdot t \cdot \lambda) \times 100\%$$

$$AQE(Total)\ \% = AQE(CO)\ \% + AQE(CH_4)\ \%$$

Where nCO and nCH_4 are the amounts of the generated electrons for CO and CH_4 during 2 h, N_A is Avogadro constant (6.022×10^{23} mol^{-1}). h is Planck constant (6.626×10^{-34} J·s). c is the speed of light (3×10^8 m/s). S is the irradiation area (m^2). I is the intensity of irradiation light (W/m^2). t is the photoreaction time (7200 s). λ is the wavelength of the monochromatic light (m).

1.3 Characterization Methods

The N_2 adsorption-desorption isotherms were collected at 77K by ASAP 2460 system, and the sample were pretreatment at 80 ℃ for 24 h. Powder X-ray diffraction (PXRD) patterns were recorded on a desktop X-ray diffractometer (MiniFlex600/600-C) with Cu Kα radiation (λ = 1.5418 Å) in the range of 2θ from 2° to 80°. Fourier transformation infrared (FT IR) spectra were acquired using a Nicolet 6700

spectrometer. X-ray photoelectron spectroscopy (XPS) was measured by Thermo ESCALAB 250 spectrometer and all elements binding energies were calibrated with the C 1s line at 284.8 eV of surface adventitious carbon. The capacity of CO_2 adsorption at 298 K was measured by ASAP 2460 system. The X-ray absorption structures at the Pb K-edge was acquired in luorescence excitation mode using a Lytle detector at the BL13SSW-XAFS beamline of the Shanghai Synchrotron Radiation Facility (SSRF). The k^3-weighted χ(k) data in k-space was Fourier-transformed to R space using Hanning windows in the Athena software to separate the EXAFS contributions from different coordination shells. The wavelet transform (WT) of EXAFS spectra was calculated using the Hama Fortran program. The XAFS fitting data was obtained using Artemis software to corroborate the local atomic structure and coordination environment of Pb atoms. Transmission electron microscopy (TEM) and field emission scanning electron microscope (FESEM) images were recorded by JEM-2100F (JEOL, Japan) and JSM-7500F, respectively. The elemental composition was evaluated using an Energy Dispersive Spectrometer (EDS). The ultraviolet-visible diffuse reflectance (UV-vis DRS) spectra were performed UV-vis spectrophotometer (Shimadzu, UV-2700i, Japan). Photoluminescence (PL) spectra were performed on Fluorescence Spectrophotometer (LabRam HR, HORIBA Jobin Yvon, France). Time-resolved photoluminescence (TRPL) spectra were examined by a fluorescence lifetime spectrophotometer (Spirit 1040-8-SHG, Newport, US) with a 490 nm laser excitation source. The energy band structure was determined by measuring ultraviolet photoelectron spectra (UPS, ESCALAB 250Xi, Thermo Fisher Scientific, USA). Electrochemical impedance spectroscopy (EIS), photocurrent measurements and Mott-Schottky were performed on a CHI-660e workstation (Shanghai Chenhua Instruments Co.), with Pt wire, Ag/AgCl (saturated KCl), and 0.1 M tetrabutylammonium hexafluorophosphate ($TBAPF_6$)/ethyl acetate solution functioning as the counter electrode, reference electrode, and electrolyte, respectively. gas chromatographic analysis was determined by GC9790II (PLF-01, Fuli instruments) equipped with a flame ionization detector (FID) and a thermal conductivity detector (TCD) column.

2. Associated content

Supporting Information

EXFAS fitting curves and WT-EXAFS spectra of Pb foil and TpBpy/$CsPbBr_3$. SEM and TEM images of TpBpy, TpBpy/$PbBr_2$ and TpBpy/$CsPbBr_3$ heterojunction. N_2 and CO_2 adsorption-desorption isotherms of TpBpy, TpBpy/$PbBr_2$ and TpBpy/$CsPbBr_3$ heterojunction. XPS spectra, and UPS spectra of $CsPbBr_3$ NCs, TpBpy, TpBpy/$PbBr_2$ and TpBpy/$CsPbBr_3$ heterojunction. XRD patterns and FTIR spectra of TpBpy/$CsPbBr_3$ heterojunction after five catalytic cycles. Steady-state PL spectra of $CsPbBr_3$ NCs, TpBpy, TpBpy/HBr, TpBpy/$PbBr_2$ and TpBpy/$CsPbBr_3$ heterojunction. Photocurrent-time response, CV curves and electrochemical impedance spectra of TpBpy, TpBpy/$PbBr_2$, and TpBpy/$CsPbBr_3$ heterojunction. In-situ DRIFTS spectra of TpBpy/$CsPbBr_3$ heterojunction. HOMO-LUMO charge-transfer transitions of TpBpy and TpBpy/$PbBr_2$. EXAFS fitting parameters. and TRPL parameters of TpBpy, TpBpy/$PbBr_2$ and TpBpy/$CsPbBr_3$ heterojunction. Comparison of CO activity and selectivity of TpBpy/$CsPbBr_3$ heterojunction with other reported photocatalysts.

Acknowledgements

We thank the Shanghai Synchrotron Radiation Facility (SSRF) for providing beam time on beamline BL13SSW for the XAS measurements. Thanks for the measurements supporting from the Centre for Materials Research and Analysis at Wuhan University of Technology (WUT).

Supplementary Figures and Tables

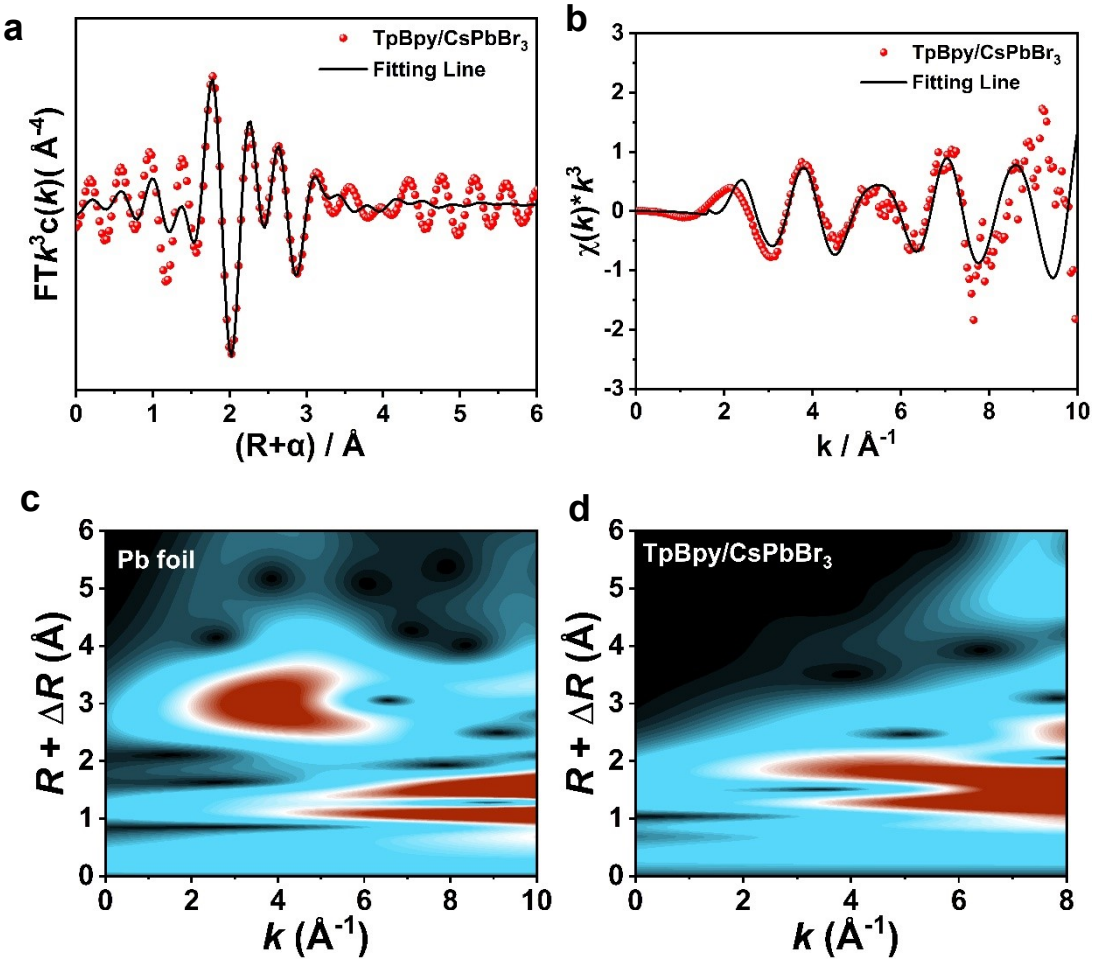

Fig. S1 EXFAS fitting curves of TpBpy/CsPbBr$_3$ (a) In R-space. **(b)** In k-space. WT-EXAFS spectra of discriminating radial distance and K-space resolution of **(c)** Pb foil and **(d)** TpBpy/CsPbBr$_3$.

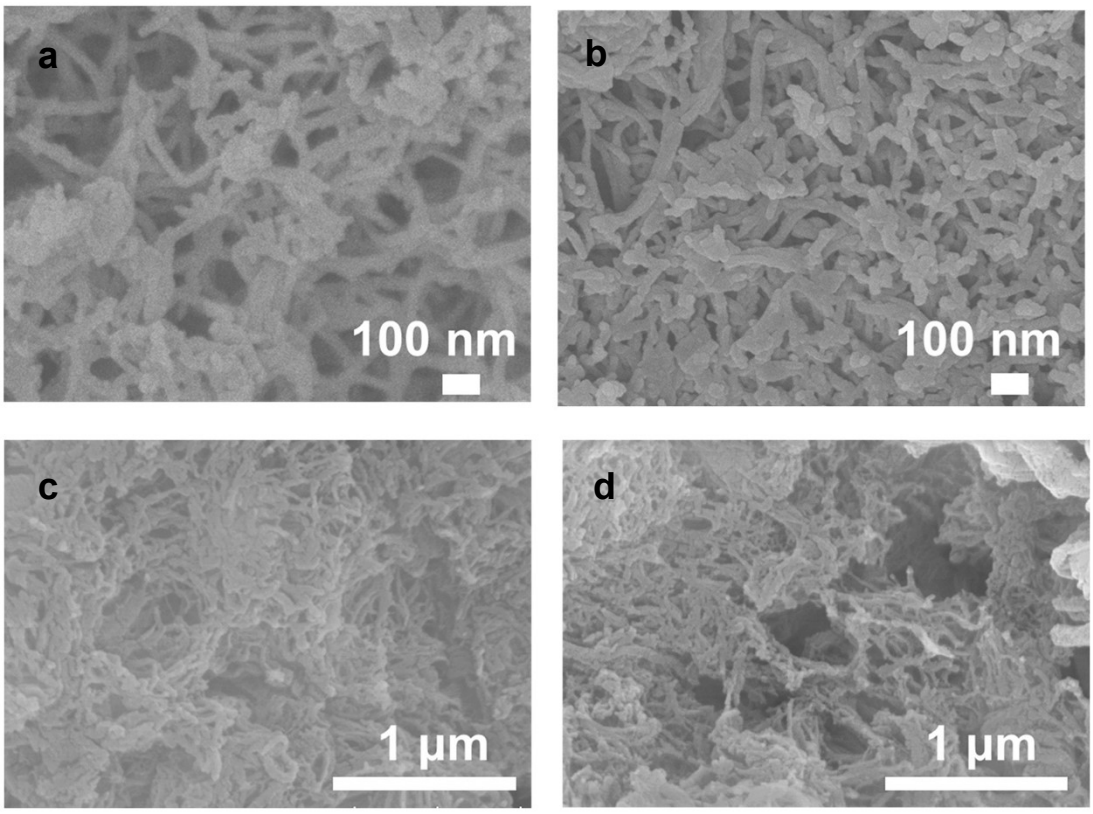

Fig. S2 SEM images of **(a)** TpBpy, **(b)** TpBpy/HBr, **(c)** TpBpy/$PbBr_2$ and **(d)** TpBpy/$CsPbBr_3$ heterojunction.

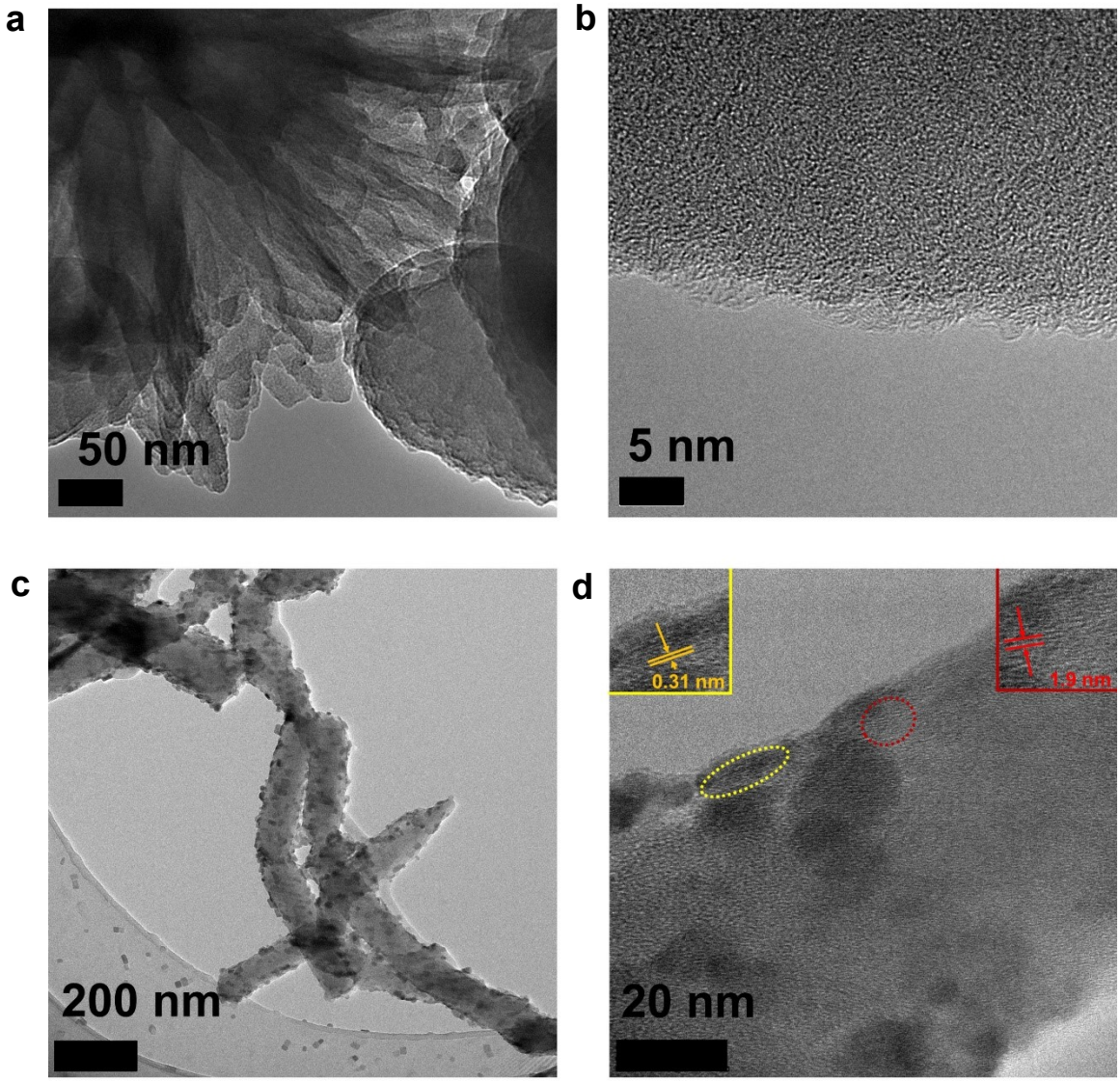

Fig. S3 TEM and HRTEM images of **(a) (b)**TpBpy, and **(c), (d)** TpBpy/$CsPbBr_3$ heterojunction**.**

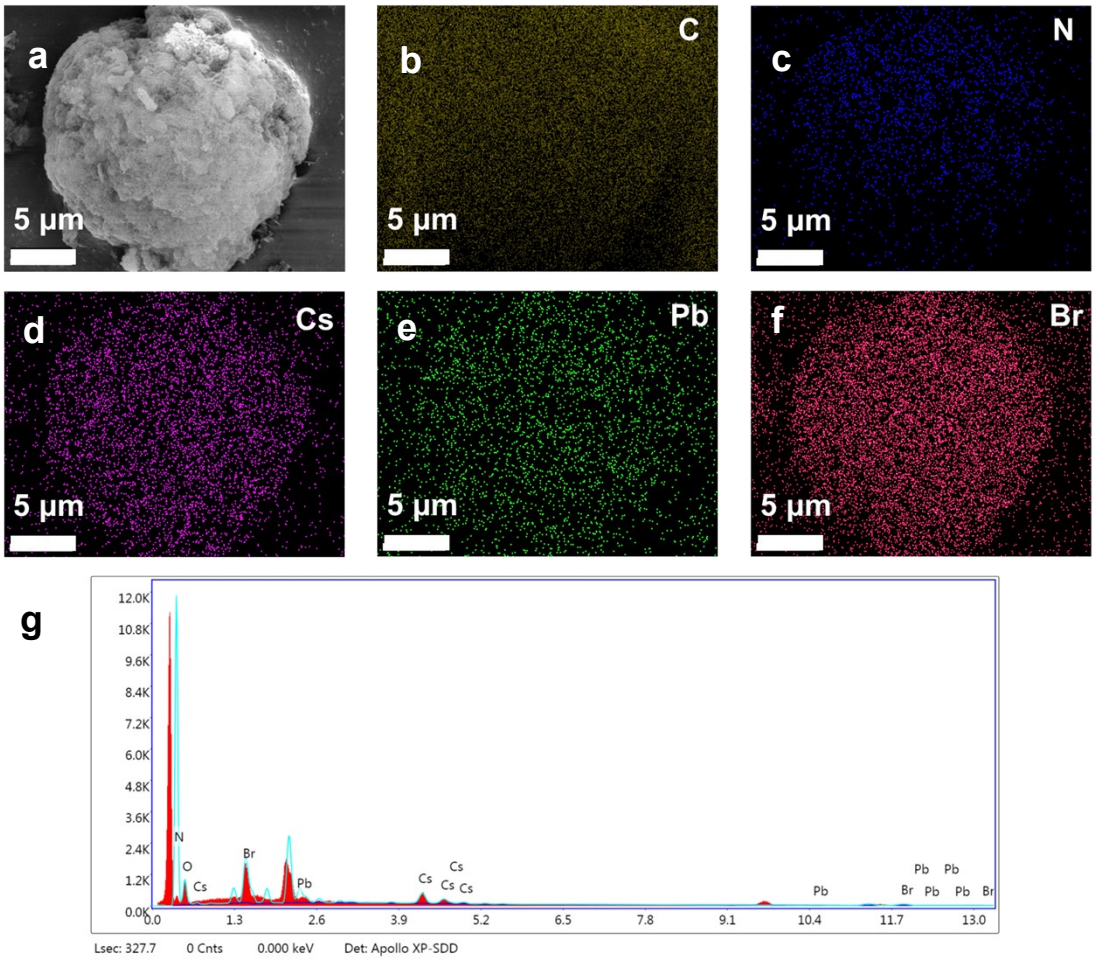

Fig. S4 SEM images of **(a)** TpBpy/$CsPbBr_3$ heterojunction, Energy dispersive X-ray (EDX) maps of TpBpy/$CsPbBr_3$ heterojunction, (b) C elements, (c) N elements, (d) Cs elements, (e) Pb elements, (f) Br elements. Scale bar: 5 μm. (g) Element distribution curve.

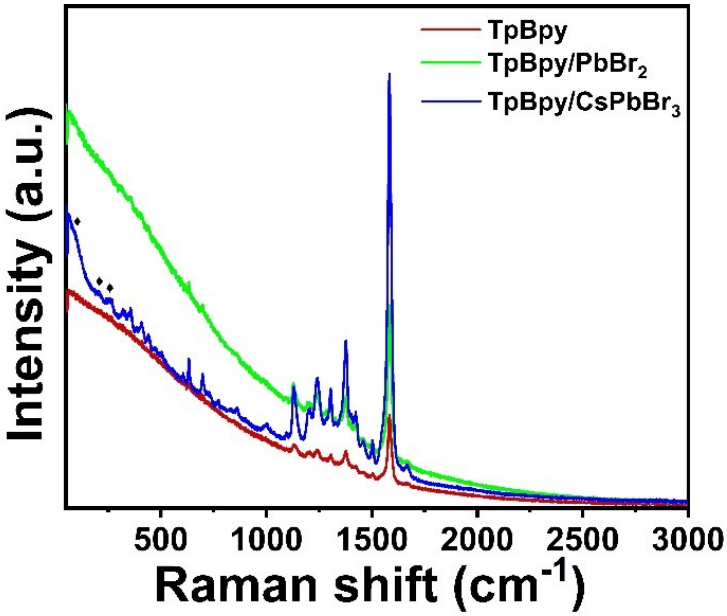

Fig. S5 Raman spectra of TpBpy, TpBpy/$PbBr_2$ and TpBpy/$CsPbBr_3$ heterojunction under 532 nm illumination.

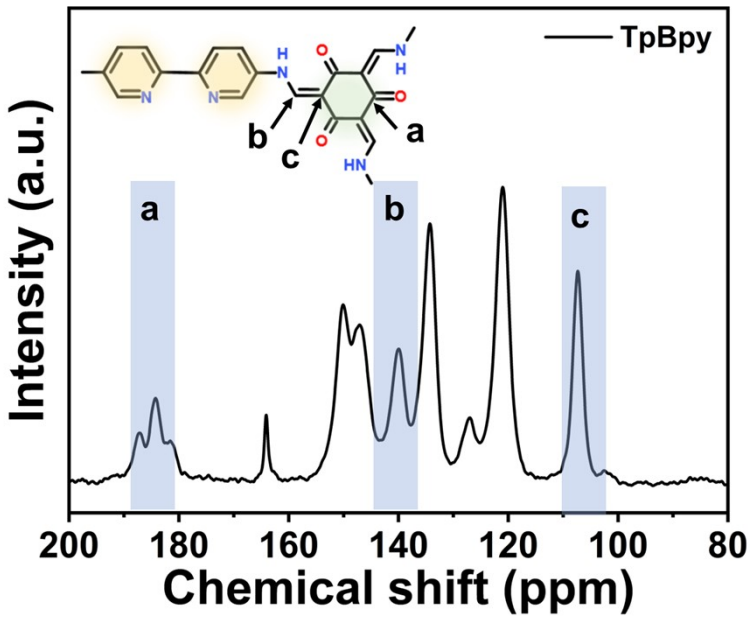

Fig. S6 Solid-state ^{13}C CP/MAS NMR spectra of TpBpy.

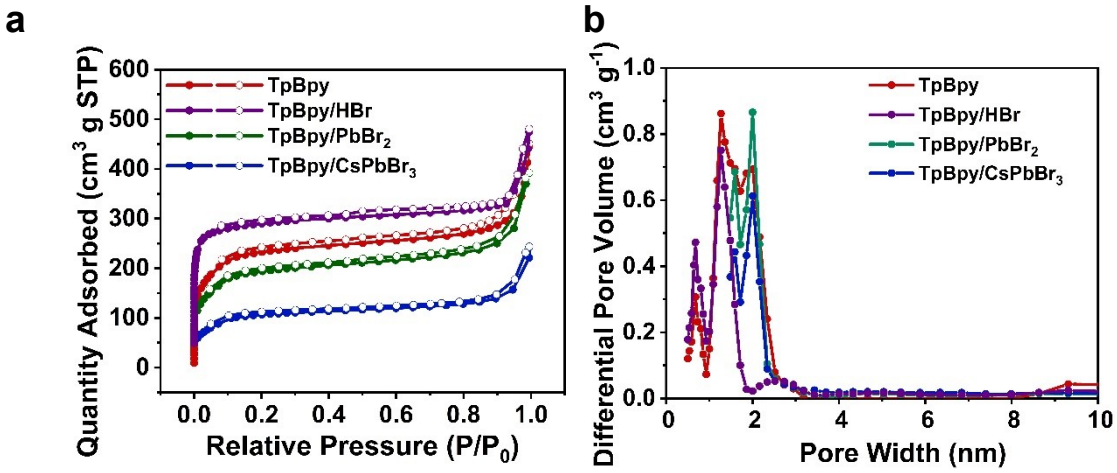

Fig. S7 N_2 adsorption data of TpBpy. (a) Gas adsorption isotherms and **(b)** pore size distributions of TpBpy, TpBpy/HBr, TpBpy/$PbBr_2$ and TpBpy/$CsPbBr_3$.

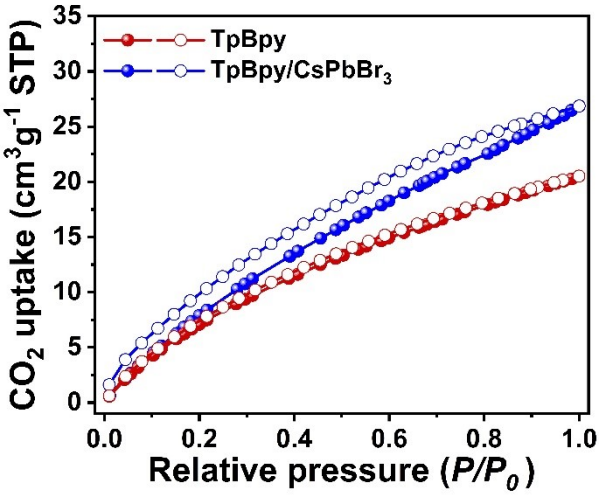

Fig. S8 CO_2 adsorption isotherms of TpBpy and TpBpy/$CsPbBr_3$ heterojunction at 298 K.

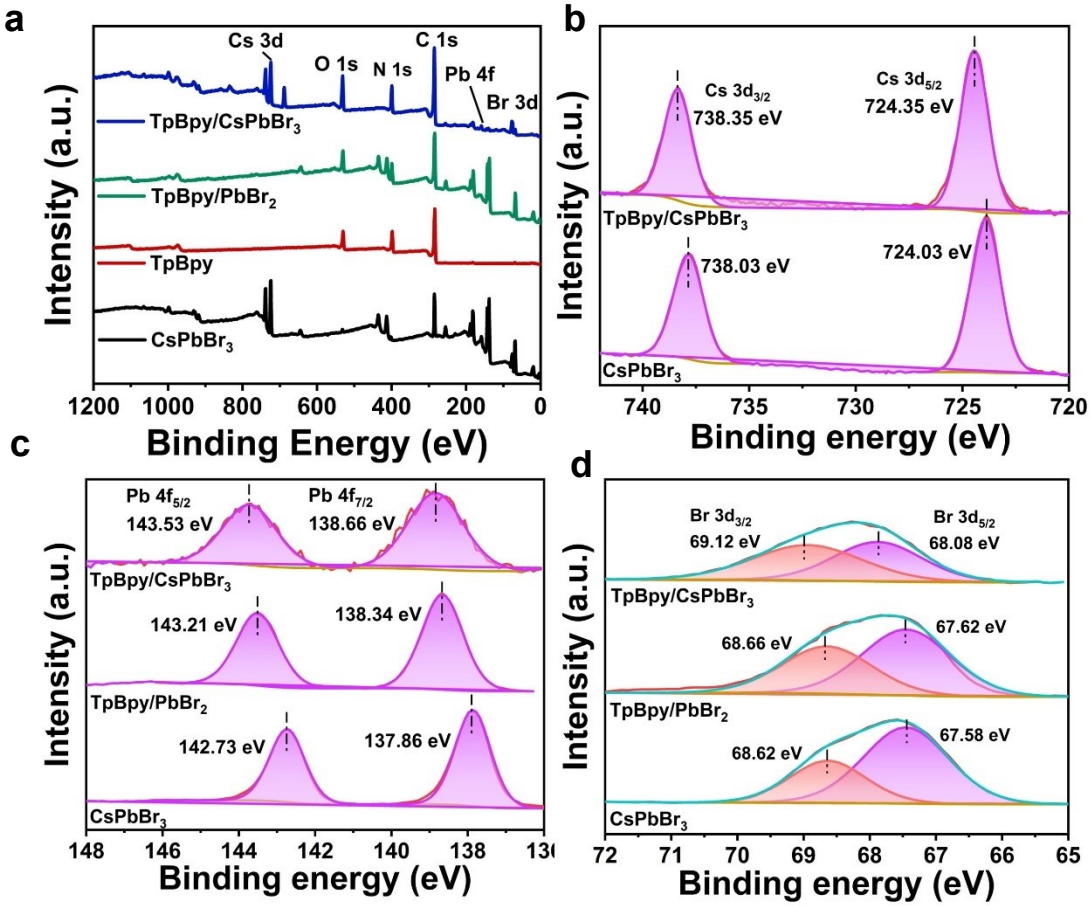

Fig. S9 XPS spectra of TpBpy, TpBpy/$PbBr_2$ and TpBpy/$CsPbBr_3$ heterojunction.

(a) Survey spectra, **(b)** Cs 3d spectra; **(c)** Br 3d spectra; **(d)** Pb 4f spectra.

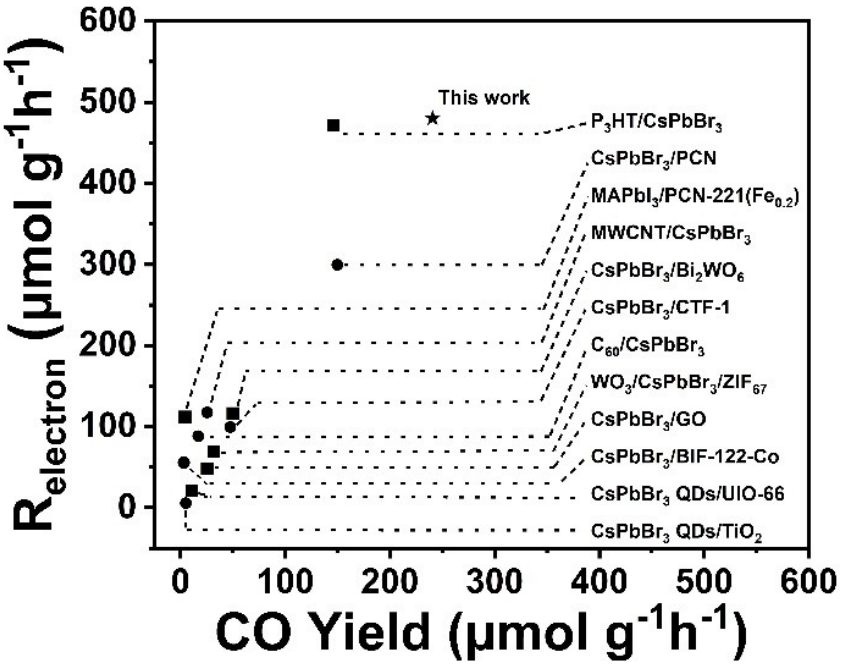

Fig. S10 CO yields and electron transfer number for TpBpy/$CsPbBr_3$ NCs in this work compared with other reported MHPs heterojunctions.

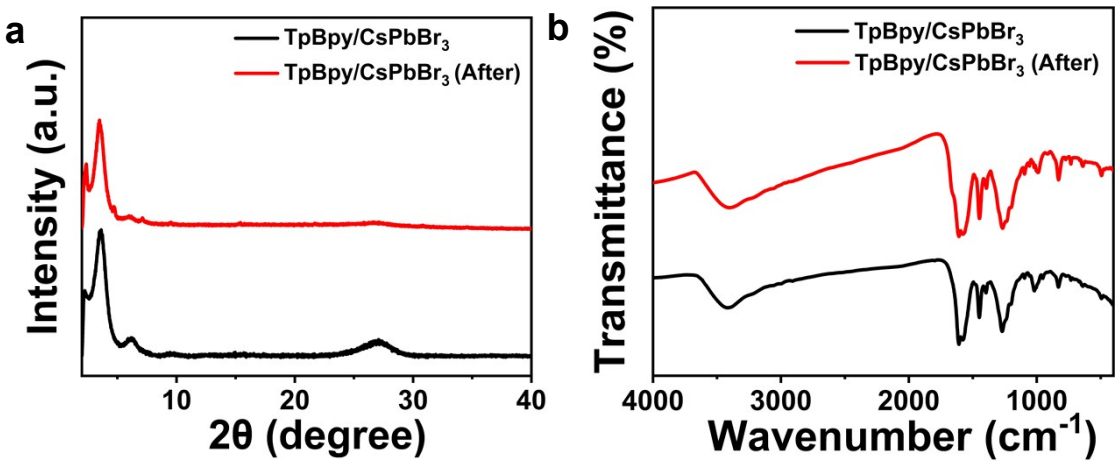

Fig. S11 (a) Powder XRD patterns and **(b)** IR spectra of TpBpy/$CsPbBr_3$ heterojunction before and after photocatalytic CO_2RR.

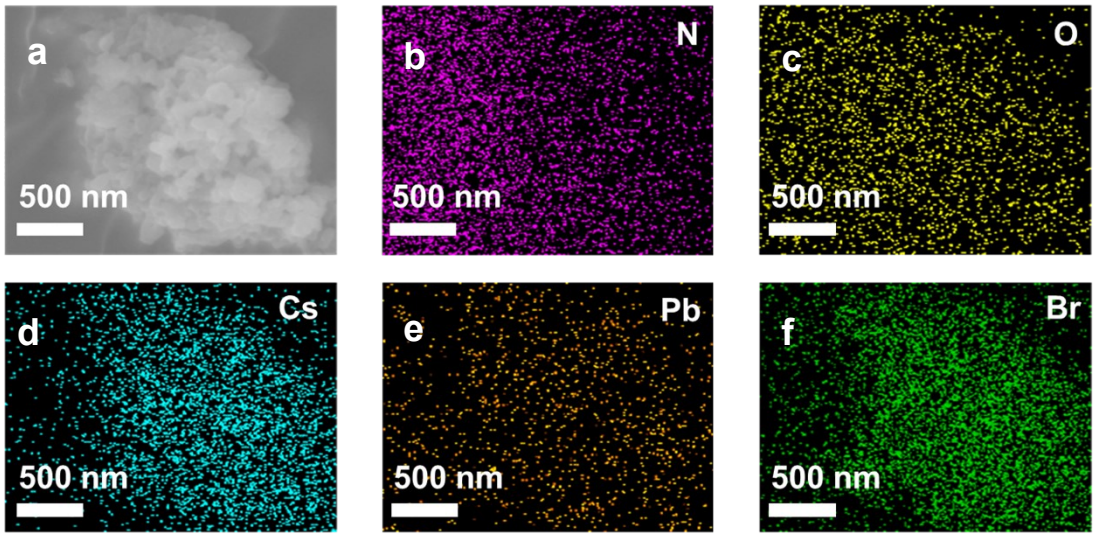

Fig. S12 (a) SEM image and (b-f) EDX maps of TpBpy/$CsPbBr_3$ heterojunction after photocatalytic CO_2RR, (b) N elements, (c) O elements, (d) Cs elements, (e) Pb elements, (f) Br elements. Scale bar: 500 nm.

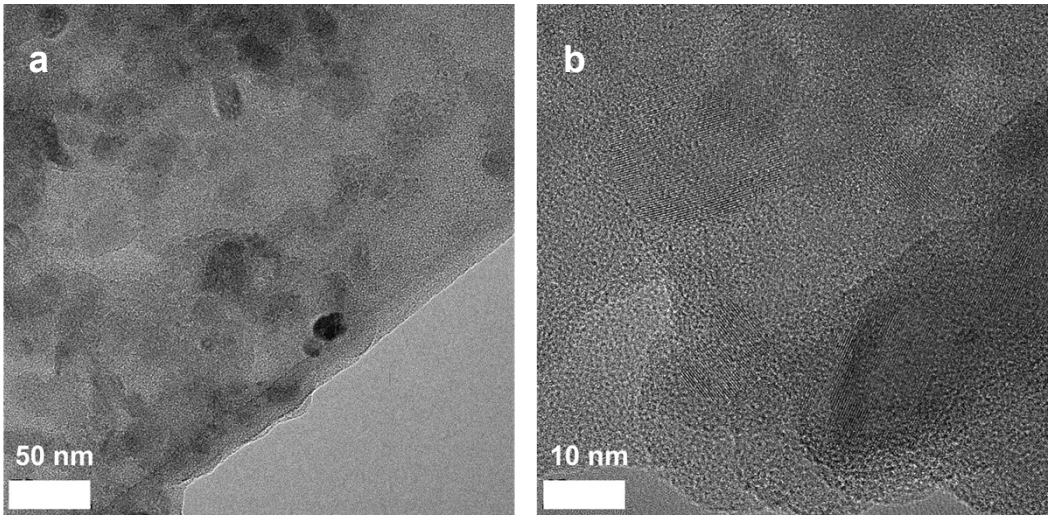

Fig. S13 (a-b) TEM images of TpBpy/$CsPbBr_3$ heterojunction after photocatalytic CO_2RR.

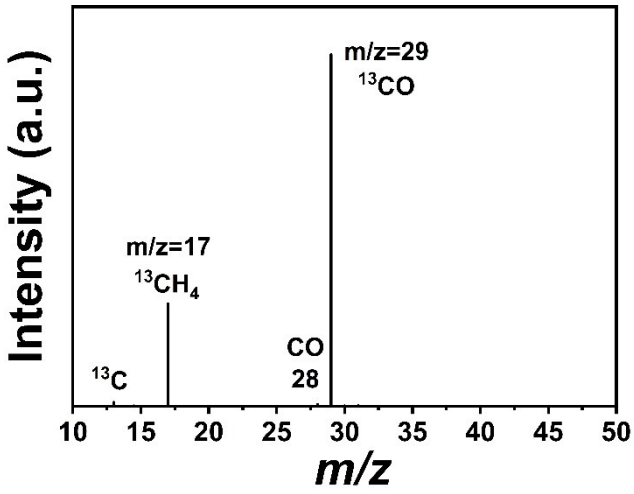

Fig. S14 Mass spectra of ^{13}CO (m/z=29) produced in the photocatalytic reduction of $^{13}CO_2$ over TpBpy/$CsPbBr_3$ heterojunction.

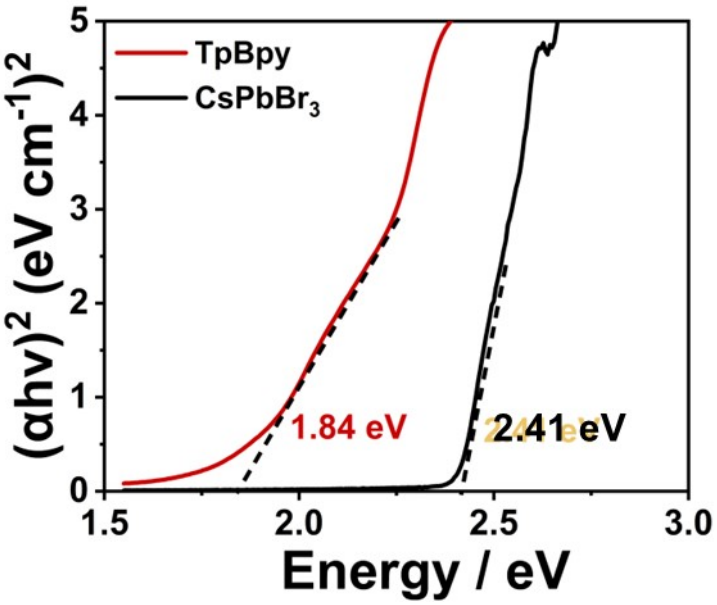

Fig. S15 Tauc plots of TpBpy and $CsPbBr_3$ NCs.

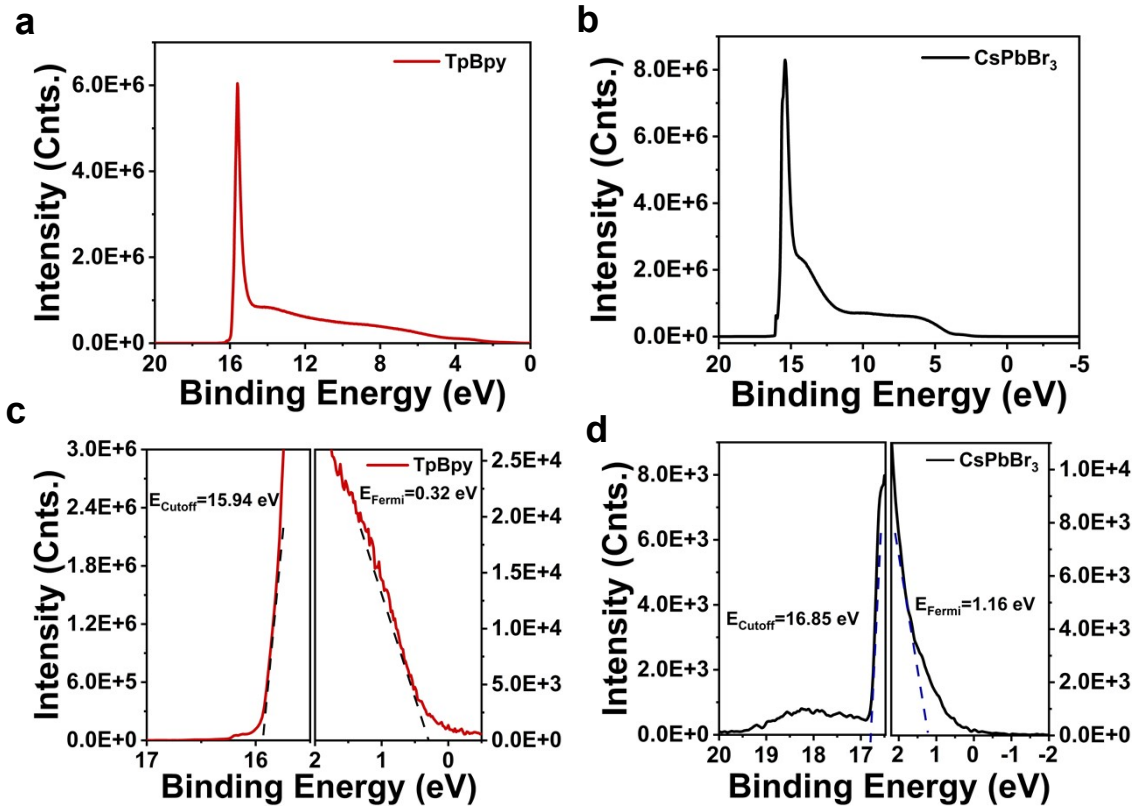

Fig. S16 Full scan UPS spectra of **(a)** TpBpy and **(b)** $CsPbBr_3$. Cut_{off} edge (left) and Fermi edge energy (right) of **(c)** TpBpy and **(d)** $CsPbBr_3$.

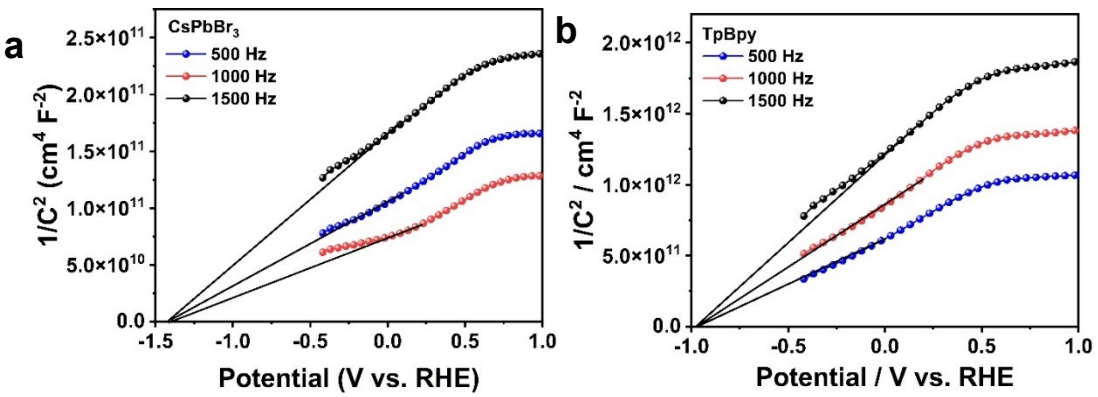

Fig. S17 Mott-Schottky plots of (a) $CsPbBr_3$ NCs and (b) TpBpy.

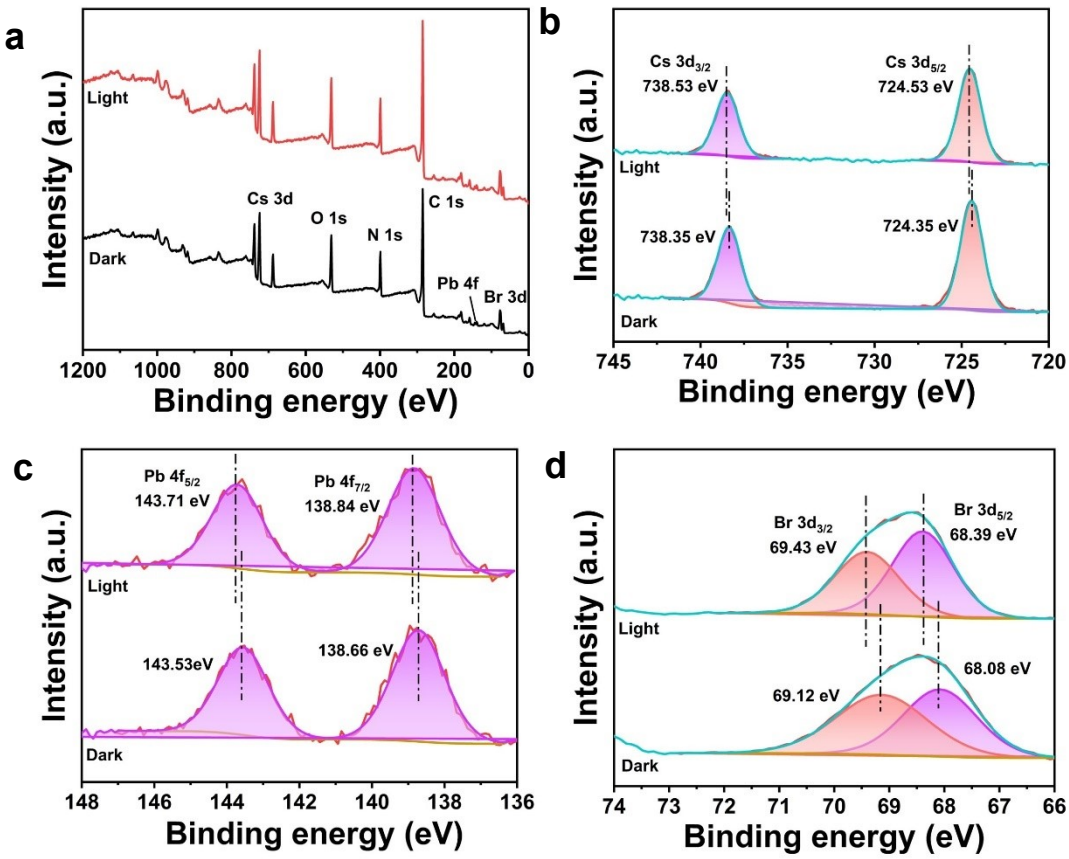

Fig. S18 Before and after light irradiation, XPS spectra of TpBpy/$CsPbBr_3$ heterojunction. (a) Survey spectra, **(b)** Cs 3d spectra; **(c)** Br 3d spectra; **(d)** Pb 4f spectra.

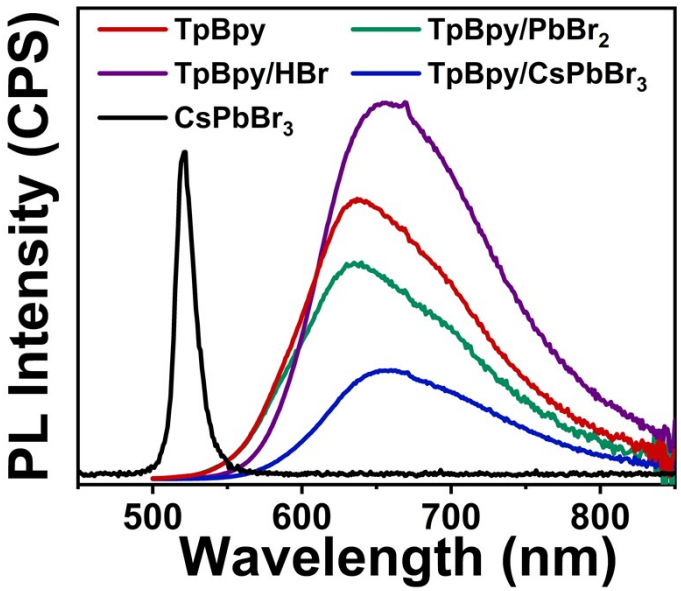

Fig. S19 Steady state PL spectra of $CsPbBr_3$, TpBpy, TpBpy/HBr, TpBpy/$PbBr_2$ and TpBpy/$CsPbBr_3$ heterojunction.

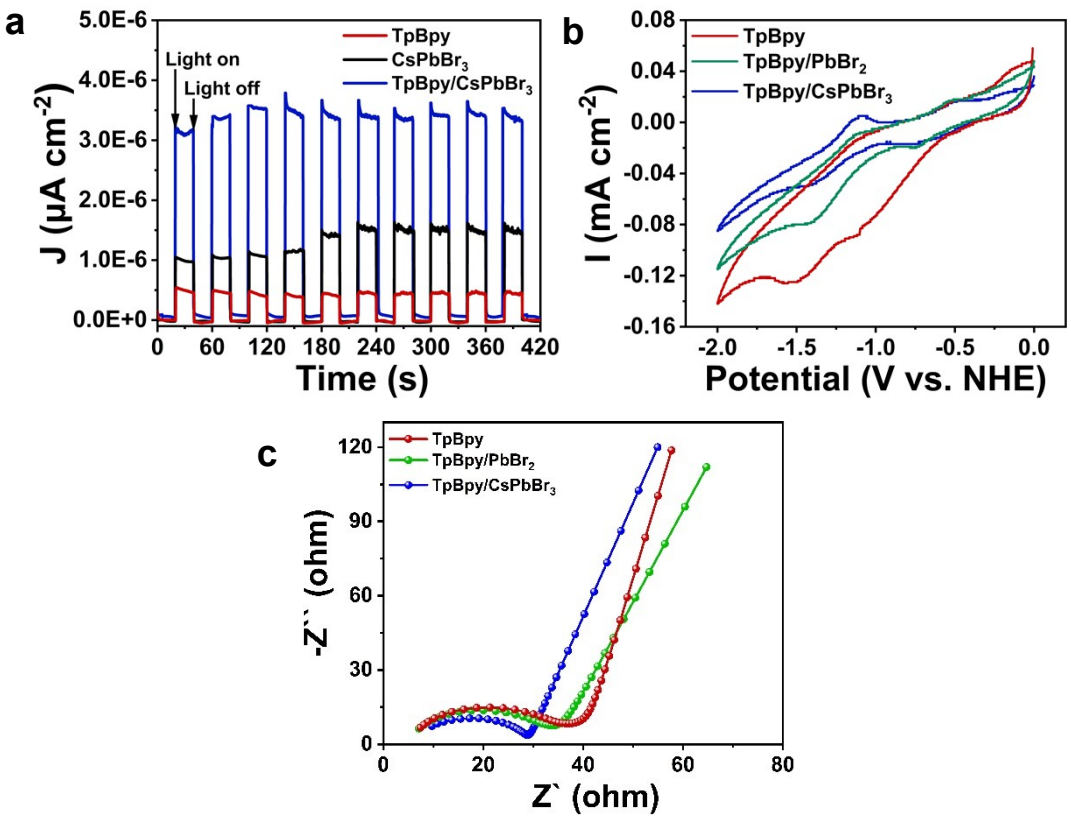

Fig. S20 (a) Photocurrent-time (I-t) response, **(b)** CV curves and **(c)** Electrochemical impedance spectra of TpBpy, TpBpy/$PbBr_2$, and TpBpy/$CsPbBr_3$ heterojunction.

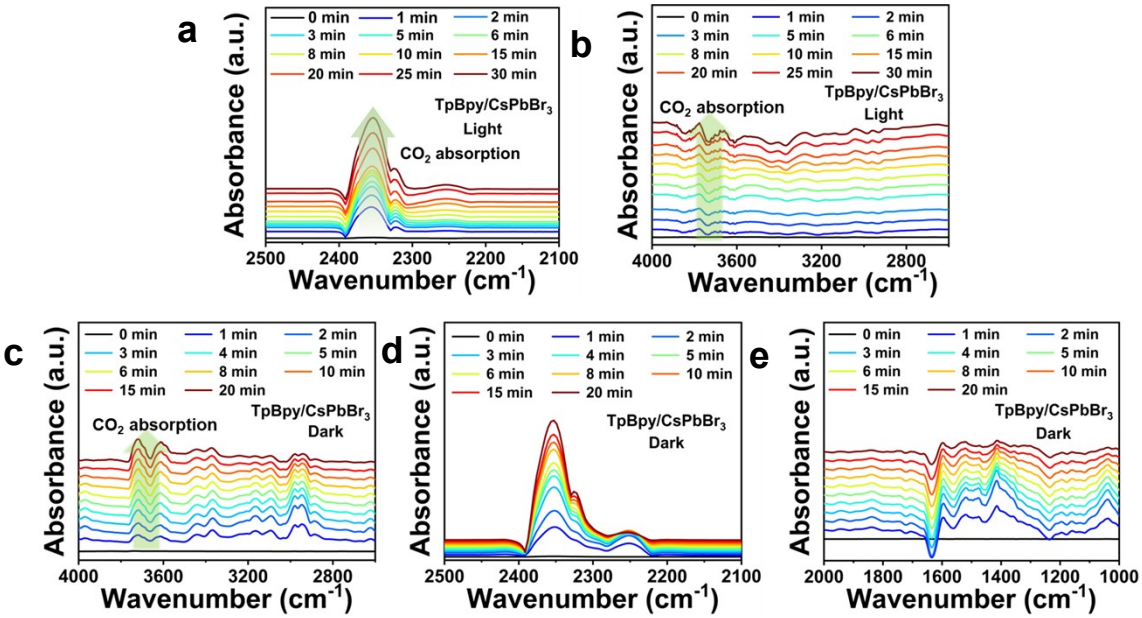

Fig. S21 In-situ DRIFTS tests for CO_2 and H_2O interaction with TpBpy/$CsPbBr_3$ heterojunction **(a-b)** in light and **(c-e)** in the dark.

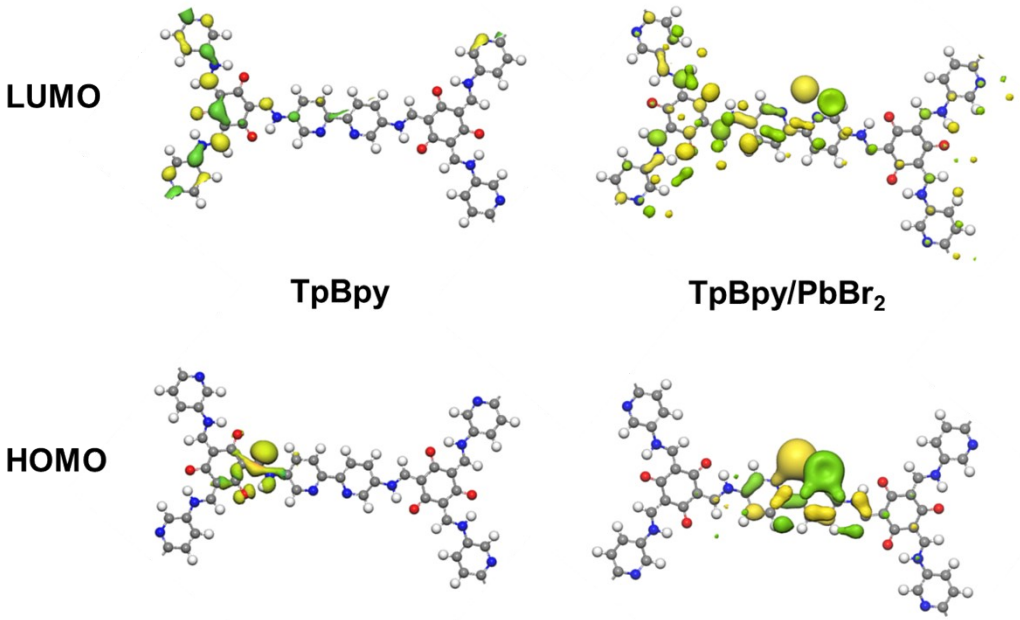

Fig. S22 HOMO-LUMO structures of TpBpy and TpBpy/$PbBr_2$.

Table S1 EXAFS fitting parameters. EXAFS curve fitting parameters of the Pb K-edge for Pb foil and TpBpy/$PbBr_2$.

Sample	Path	N	R/Å	σ^2/Å^2	ΔE_0/eV	R-factor/%
Pb foil	Pb-Pb	12	3.378	0.003	2.4	0.003
TpBpy/$PbBr_2$	Pd-N	2	2.024	0.002	4.2	0.004
	Pb-Br	2	2.761	0.005	4.2	0.004

Table S2 Performance comparison. Photoreduction CO_2 performance of TpBpy/$CsPbBr_3$ NCs was compared with other reported MHPs heterojunctions.

Photocatalysts	Reaction condition	Light source	Products/ μmol g^{-1} h^{-1}	$R_{electrons}$/ μmol g^{-1} h^{-1}	CO Selectivity / %
TpBpy/$CsPbBr_3$	ACN+H_2O	300 W Xe lamp AM 1.5G λ≥ 420nm	**CO: 239.46 CH_4: 0.21**	**480.6**	**99.66**
$CsPbBr_3$ QD/g-C_3N_4[1]	ACN+H_2O	300 W Xe lamp λ≥ 420nm	/	148.9	/
$CsPbBr_3$ QD/TiO_2[2]	ACN+H_2O	300 W Xe lamp	CO: 5.98 H_2: 1.32	9.02	/
C_{60}/$CsPbBr_3$[3]	ACN+H_2O	300 W Xe lamp λ≥ 420nm	CO: 17.8 CH_4: 6.8	90	39.56
$CsPbBr_3$-$SOBr_2$/g-C_3N_4[4]	EA+H_2O	300 W Xe lamp	/	190	/
P3HT/$CsPbBr_3$[5]	ACN+H_2O	300 W Xe lamp λ≥ 420nm	CO: 145.45 CH_4: 23.05	475.3	61.2
$CsPbBr_3$ QD/UIO-66[6]	ACN+H_2O	300 W Xe lamp λ≥ 420nm	CO: 8.21 CH_4: 0.26	18.5	88.76
$CsPbBr_3$/BIF-122-Co[7]	EA+H_2O	300 W Xe lamp λ≥ 420nm	CO: 5.07 CH_4: 5.25	52.14	19.45
$MAPbI_3$/PCN-221(Fe0.2)[8]	ACN/EA+H_2O	300 W Xe lamp λ≥ 400nm	CO: 4.16 CH_4: 13	112.32	7.41
$CsPbBr_3$/CTF-1[9]	EA	300 W Xe lamp λ≥ 400nm	CO: 48.2	96.4	
MWCNT/$CsPbBr_3$[10]	ACN	300 W Xe lamp λ≥ 420nm	CO: 24.58 CH_4: 8.38	116.19	
$CsPbBr_3$ QD/Bi_2WO_6[11]	EA+H_2O	300 W Xe lamp λ≥ 400nm	CO: 50.3	114.4	
$CsPbBr_3$ QD/PCN[12]	ACN+H_2O	300 W Xe lamp λ≥ 420nm	CO: 148.9	297.8	
$CsPbBr_3$ QD/GO[13]	EA	100 W Xe lamp AM 1.5G	CO: 23.7	47.4	99.3%
WO_3/$CsPbBr_3$/ZIF-67[14]	Solid-gas system	150-W Xe lamp AM 1.5G	CO: 33.13 CH_4: 0.50	70.22	

Table S3 Fitted TR-PL lifetimes of the $CsPbBr_3$ QDs, TpBpy, TpBpy/$PbBr_2$ and TpBpy/$CsPbBr_3$ heterojunction.

Sample	τ_1 (ns)	A_1	τ_2 (ns)	A_2	τ_3(ns)	A_3	τ_{av} (ns)
$CsPbBr_3$	3.55	0.39	11.79	0.34	31.86	0.27	6.57
TpBpy	0.79	0.24	0.16	0.72	2.28	0.04	0.15
TpBpy/$PbBr_2$	0.09	0.71	0.30	0.34	1.05	0.11	0.10
TpBpy/$CsPbBr_3$	0.05	0.45	0.26	0.43	0.94	0.12	0.10

Reference

[1] M. Ou, W. G. Tu, S. M. Yin, W. N. Xing, S. Y. Wu, H. J. Wang, S. P. Wan, Q. Zhong, R. Xu, *Angew. Chem. Int. Ed.*, 2018, **130**, 13758-13762.

[2] F. Y. Xu, K. Meng, B. Cheng, S. Y. Wang, J. S. Xu, J. G. Yu, *Nat. Commun.*, 2020, **11**, 4613.

[3] Z. J. Zhang, M. Y. Shu, Y. Jiang, J. Y. Xu, *Chem. Eng. J.*, 2021, **414**, 128889.

[4] Q. Zheng, J. Wang, X. Li, Y. Bai, Y. P. Li, J. C. Wang, Y. Y. Shi, X. Y. Jiang, Z. Q. Li, *ACS Mater. Lett.*, 2022, **4**, 1638-1645.

[5] L. L, Z. J. Zhang, C. Ding, J. Y. Xu, *Chem. Eng. J.*, 2021, **419**, 129543.

[6] S. p.Wan, M. Ou, Q. Zhong, X. N. Wang, *Chem. Eng. J.*, 2019, **358**, 1287-1295.

[7] Z. Y. Chen, Q. L. Hong, H. X. Zhang, J. Zhang, *ACS Appl. Energy Mater.*, 2022, **5**, 1175-1182.

[8] L. Y. Wu, Y. F. Mu, X. X. Guo, W. Zhang, Z. M. Zhang, M. Zhang, T. B. Lu, *Angew. Chem. Int. Ed.*, 2019, **58**, 9491-9495.

[9] Q. Wang, J. Wang, J. C. Wang, X. Hu, Y. Bai, X. H. Zhong, Z. Q. Li, *ChemSusChem*, 2021, **14**, 1131-1139.

[10] M. Y. Shu, Z. J. Zhang, Z. L. Dong, J. Y. Xu, *Carbon*, 2021, **182**, 454-462.

[11] J. C. Wang, J. Wang, N. Y. Li, X. Y. Du, J. Ma, C. H. He, Z. Q. Li, *ACS Appl. Mater. Interfaces*, 2020, **12**, 31477-31485.

[12] M. Ou, W. g. Tu, S. M. Yin, W. N. Xing, S. Y. Wu, H. J. Wang, S. P. Wan, Q. Zhong, R. Xu, *Angew. Chem. Int. Ed.*, 2018, **57**, 13570-13574.

[13] Y. F. Xu, M. Z. Yang, B. X. Chen, X. D. Wang, H.Y. Chen, D. B. Kuang, C. Y. Su, *J. Am. Chem. Soc.*, 2017, **139,** 5660-5663.

[14] Y. J. Dong, Y. Jiang, J. F. Liao, H. Y. Chen, D. B. Kuang, C. Y. Su, *Sci. China, Mater.*, 2022, **65**, 1550-1559.